PHYSICAL REVIEW B **93**, 045104 (2016)

Spin-orbit coupling induced band structure change and orbital character of epitaxial IrO_2 films

Woo Jin Kim,[1,2] So Yeun Kim,[1,2] Choong H. Kim,[1,2] Chang Hee Sohn,[1,2] O. B. Korneta,[1,2] Seung Chul Chae,[3] and Tae Won Noh[1,2,*]

[1]*Center for Correlated Electron Systems, Institute for Basic Science (IBS), Seoul 151-747, Republic of Korea*
[2]*Department of Physics and Astronomy, Seoul National University, Seoul 151-747, Republic of Korea*
[3]*Department of Physics Education, Seoul National University, Seoul 151-747, Republic of Korea*

(Received 4 November 2015; published 6 January 2016)

We investigated the electronic structure of IrO_2 to address the controversy regarding spin-orbit coupling (SOC) effects in metallic 5*d* transition-metal oxides. Two issues have come to the forefront: (1) SOC effects on electronic structure and physical properties of IrO_2 and (2) the possible formation of a novel ground state in this material, the $J_{\text{eff}} = 1/2$ state. To better understand the SOC mechanism, we grew epitaxial IrO_2 films whose *dc* resistivity values were comparable with those of a single crystal. We obtained polarization-dependent optical and x-ray absorption spectra (XAS) and compared these results with those acquired using the generalized gradient approximation (GGA) and GGA + SOC calculations. From the optical spectra, peak structures were identified at 0.4 and 2.0 eV, which could only be explained using the GGA + SOC calculation. This suggests that SOC plays an important role in the electronic structure of IrO_2. From the polarization-dependent O 1*s* XAS spectra, we observed that the empty state near the Fermi level lacks involvement of an Ir d_{xy} orbital. Despite the importance of SOC in IrO_2, the $J_{\text{eff}} = 1/2$ state does not form in metallic IrO_2.

DOI: 10.1103/PhysRevB.93.045104

I. INTRODUCTION

Spin-orbit coupling (SOC) in iridates has attracted much attention due to their intriguing novel ground states as well as potential applications. For example, in Sr_2IrO_4, the SOC induces nontrivial electronic properties, such as 5*d* Mott insulators [1–3]. With large SOC and electron-electron correlations, pyrochlore iridates are promising candidate materials to realize novel topological phases, such as Weyl semimetals and axion insulators [4–6]. Na_2IrO_3 is considered to be a useful system for topological quantum computation [7].

Recently, a metallic 5*d* IrO_2, one of the simplest forms of iridium compounds, has gained particular attention among iridates. It has been proposed that IrO_2 can be used as a very good spin detector material, thanks to a large spin Hall angle due to pronounceable SOC and large resistivity [8]. More recently, it was shown that the dominant carrier type can be controlled in the nonsymmorphic IrO_2 films by applied magnetic-field direction [9]. Obviously, a detailed understanding of the role of SOC in the electronic structure of this compound is essential for such novel applications.

The importance of SOC in the electronic structure of IrO_2 has been debated for some time. In the early days, physical properties of IrO_2 had been explained without considering SOC [10–12]. In the 1970s, Graebner *et al.* measured the Fermi-surface topology of IrO_2 by magnetothermal oscillations [13]. To explain the experimental data, Mattheiss used the Slater-Koster linear-combination-of-atomic-orbitals calculation method and found that the Fermi-surface topology was significantly altered by SOC effects [14]. Following these earlier studies, the role of SOC in the electronic structure of IrO_2 has been investigated using a variety of spectroscopic techniques [15–20] and first-principles calculations [9,20–22]. However, the debate on precisely how SOC affects the electronic structure of metallic IrO_2 still remains unsettled.

Another interesting issue in metallic IrO_2 is the possible formation of a novel ground state, called the $J_{\text{eff}} = 1/2$ state. It has been established recently that the $J_{\text{eff}} = 1/2$ state can form as a novel ground state in the known insulating iridates, such as Sr_2IrO_4, $Sr_3Ir_2O_7$, and Na_2IrO_3 [1,2,23–25]. In the presence of a large cubic crystal field, the 5*d* orbitals are split into t_{2g} and e_g levels, and all five electrons should occupy the t_{2g} levels. When SOC is large, t_{2g} levels split into effective total angular momentum states: fourfold $J_{\text{eff}} = 3/2$ and twofold $J_{\text{eff}} = 1/2$ states. Because the energies of the $J_{\text{eff}} = 1/2$ states are higher than those of the $J_{\text{eff}} = 3/2$ states, half of the $J_{\text{eff}} = 1/2$ states should be occupied [1]. With moderate on-site Coulomb interaction U, it is possible to form a Mott insulator with the $J_{\text{eff}} = 1/2$ ground state, which has been confirmed in numerous 5*d* compounds [1,2,23–25]. Some studies claim that this intriguing $J_{\text{eff}} = 1/2$ state is applicable even in metallic IrO_2, although the presence of this state is yet to be confirmed experimentally [9,19–21]. However, due to the itinerant nature and relatively large bandwidth of metallic compounds, other groups argue that the $J_{\text{eff}} = 1/2$ state is not relevant in IrO_2 [26–28].

In this paper, we investigated the importance of SOC and the possible formation of the $J_{\text{eff}} = 1/2$ state in IrO_2. To elucidate the roles of SOC, we grew high-quality epitaxial thin films of IrO_2. We performed optical and x-ray absorption spectroscopy (XAS) measurements on our samples and compared the data with first-principles calculations with and without SOC contribution. From our optical measurements, we determined that SOC should play an important role in the electronic structure of IrO_2, especially near the Fermi surface. SOC causes the degenerate bands to split, especially along the *ZUR* line. However, despite its importance, we do not observe the formation of the novel $J_{\text{eff}} = 1/2$ state in the metallic IrO_2 from our XAS measurements. The possible orbital state of the unoccupied band near the Fermi energy

*Electronic address: twnoh@snu.ac.kr

(E_F) would be a mixed state of π-bonding d_{yz} and d_{zx} orbitals.

II. EXPERIMENTAL DETAILS

To fabricate epitaxial IrO_2 films, we used pulsed laser deposition. We irradiated a single-phase IrO_2 polycrystalline target with a KrF excimer laser (repetition rate: 3 Hz); the laser fluence at the target surface was $\sim$1 J cm^{-2}. The distance between the target and the substrate was maintained at $\sim$50 mm. To grow the IrO_2 films with the (100) direction normal to the substrate, we used a single-crystal TiO_2 (100) substrate. The optimal conditions for high-quality IrO_2 films were stabilized at a substrate temperature T_g of 400 °C under an oxygen pressure of 50 mTorr. Temperature-dependent resistivity was measured by the conventional four-probe technique from 2 to 300 K in a physical property measurement system (Quantum Design).

We used reflectance and spectroscopic ellipsometry measurements to obtain the real parts of *b*- and *c*-axis optical conductivity $\sigma_{1b}(\omega)$ and $\sigma_{1c}(\omega)$. For 0.74–4 eV, $\sigma_{1b}(\omega)$ and $\sigma_{1c}(\omega)$ were directly measured using a V-Vase ellipsometer (J.A. Woollam Co., Lincoln, NE). From 6 to 600 meV, we measured the near-normal reflectance with polarized light parallel to *b* and *c* crystallographic axes of the sample. We used an *in situ* gold evaporation technique to minimize experimental error [29]. Then we fitted both the low-energy reflectance spectra and the high-energy $\sigma_{1b}(\omega)$ and $\sigma_{1c}(\omega)$ using a model with one Drude peak and four Lorentz oscillators. This fitting process provided us experimental $\sigma_{1b}(\omega)$ and $\sigma_{1c}(\omega)$ in the broad energy range. Density functional theory calculation was performed with the generalized gradient approximation (GGA) without and with SOC as implemented in the ELK code. In addition, the linear optical dielectric responses have been calculated within the random-phase approximation.

We performed polarization-dependent O 1*s* XAS measurements at the 2A beamline at the Pohang Light Source (PLS) in the total electron yield mode. To ensure that additional iridium oxidation did not occur on the surface during sample transfer, we performed *in situ* x-ray photoelectron spectroscopy (XPS) and *ex situ* XPS studies of Ir 4*f* and 5*p* core levels of IrO_2 on the same sample. Even after long exposure to air, the *ex situ* XPS spectra remained the same as the *in situ* XPS spectra. And they agreed with the XPS data of bulk IrO_2 [26]. Therefore, our O 1*s* XAS spectra contain information only for IrO_2, not those from any other oxidation states.

III. RESULTS AND DISCUSSION

A. Structural characterization and transport property

We used x-ray diffraction (XRD) to confirm that our IrO_2 films were epitaxially grown with lattice parameters close to those of the bulk compound. Figure 1(b) shows the XRD $\theta-2\theta$ scans of our IrO_2 film, indicating that the film was epitaxially grown without any impurity phases. A film thickness of 11 nm has been estimated based on interference fringes of the film diffraction peak. To measure the in-plane lattice constants of the film and the substrate, we used x-ray reciprocal space mapping (X-RSM). Figures 1(c) and 1(d) show X-RSM data around the (301) and (310) Bragg reflections, respectively,

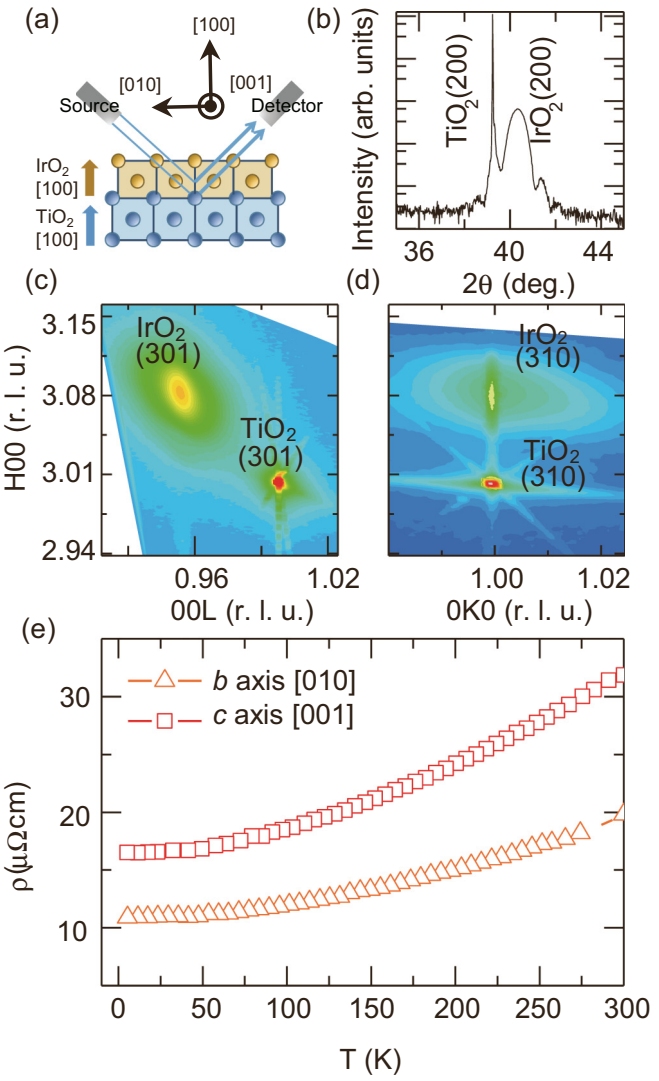

FIG. 1. (a) X-ray sideways geometry to probe the (200) Bragg peak in the thin film/substrate. (b) X-ray diffraction pattern of IrO_2 grown on a (100) TiO_2 substrate. (c) Reciprocal space mapping of (301) IrO_2. (d) Reciprocal space mapping of (310) IrO_2. (e) Temperature dependence of the resistivity of an IrO_2 thin film along [010] and [001] corresponding to the *b* axis and *c* axis, respectively.

of both the IrO_2 film and the TiO_2 substrate. From the experimental *H*, *K*, and *L* values, the lattice constants of our film are estimated to be $a = 4.47$, $b = 4.58$, and $c = 3.10$ Å. This result indicates that the film is actually partially tensile strained about 1.7% along the *b*-axis direction, whereas it is compressive strained about 1.6% along the *c*-axis direction. Our X-RSM data also show that the $a-c$ axes of the IrO_2 film are aligned with the [100], [010], and [001] axes of the TiO_2 substrate, respectively.

The resistivity ρ of our epitaxial IrO_2 film decreases with temperature, in consistence with a metallic ground state. Note that IrO_2 has anisotropic ρ. We prepared two kinds of electrodes which were aligned along the *b* or *c* axes and measured the direction-dependent ρ. Figure 1(e) shows the temperature-dependent ρ along the [010] and [001] directions: the anisotropic values close to those of single crystals. At

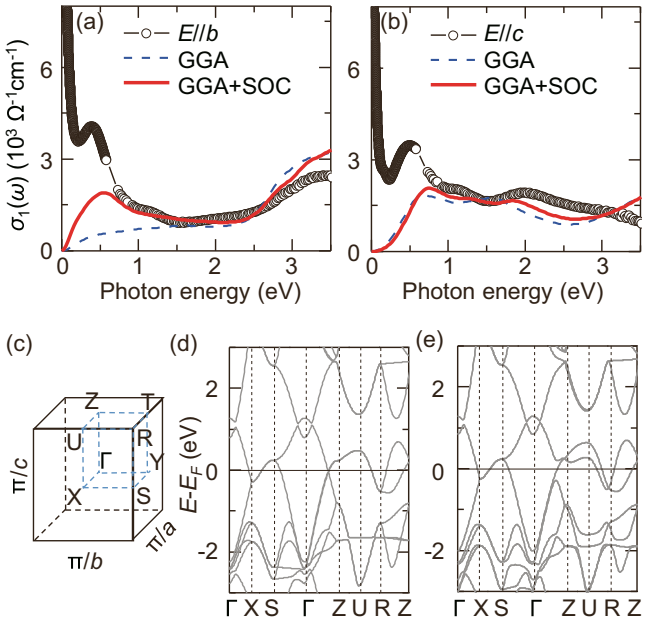

FIG. 2. (a) Experimental optical conductivity spectra of the IrO_2 b axis [010] (black empty circle) and theoretically computed interband component of the optical conductivity values based on GGA (blue dashed line) and GGA + SOC (red solid line). (b) Experimental optical conductivity spectra of the IrO_2 c axis [001] and theoretically computed interband component of the optical conductivity values based on GGA (blue dashed line) and GGA + SOC (red solid line). (c) Brillouin zone of an IrO_2 film. (d) Band dispersion computed within the GGA approximation. (e) Band dispersion computed within the GGA + SOC approximation.

300 K, ρ's for the c and b axes were measured to be 32 and 20 $\mu\Omega$ cm, respectively; the values similar to those of a single crystal, i.e., 49 and 28 $\mu\Omega$ cm, respectively [11]. However, the residual-resistance ratio (RRR) $\rho(2\,\mathrm{K})/\rho(300\,\mathrm{K})$ values of our film were around 2 for both ρ_b and ρ_c. These values are smaller than those of single crystals but comparable to the values of epitaxial films [9,11] and higher than those previously reported for polycrystalline films [30–36]. The small RRR value might come from lots of misfit dislocations, which inevitably resulted during the growth of the partially relaxed films.

B. Optical spectroscopy and first-principles calculations

We observed the free-carrier response and several interband transitions in $\sigma_{1b}(\omega)$ and $\sigma_{1c}(\omega)$. The open circles in Figs. 2(a) and 2(b) display the $\sigma_{1b}(\omega)$ and $\sigma_{1c}(\omega)$, respectively, of our IrO_2 film. Below 0.2 eV, both spectra show the Drude response, indicating a metallic state. The inverse values of $\sigma_{1b}(0)$ and $\sigma_{1c}(0)$ from fitting are about 64 and 92 $\mu\Omega$ cm, respectively, which are in good agreement with those from the direct dc resistivity measurements. In $\sigma_{1b}(\omega)$, we observed two strong peaks around 0.4 and 3.5 eV and two small peaks around 1.1 and 2.0 eV. In $\sigma_{1c}(\omega)$, we observed two strong peaks around 0.5 and 2.0 eV and an easily discernible peak at ∼1.1 eV. Earlier optical data on the polycrystalline IrO_2 films reported peak structures around 0.4, 0.9, 1.8, and 3.6 eV, similar to our observations [17] but could not resolve optical anisotropy. In the earlier studies, all of the peaks below 2.0 eV were assigned to $d-d$ transitions.

The results of GGA and GGA + SOC calculations using lattice constants of IrO_2 film are shown in Figs. 2(d) and 2(e), respectively. We have confirmed that the differences between the calculation results from bulk lattice constants and those of the film are negligible. Although the general band dispersions in the wide energy regions are similar to each other, SOC causes the degenerate bands to split, especially along the ZUR line. Such a splitting could result in additional optical transitions, which might be missing when SOC is not turned on. The dashed and solid lines in Figs. 2(a) and 2(b) are the theoretically computed interband component of the $\sigma_1(\omega)$ values with and without SOC, respectively. $\sigma_1(\omega)$ values from the experiments show better agreement with those from GGA + SOC than GGA. Figure 2(a) shows peaks around 0.5, 1.2, and 1.9 eV, in good agreement with experimental $\sigma_1(\omega)$. Figure 2(b) also shows reasonable agreement between experimental and GGA + SOC calculations except the lowest peak position, which might be due to the omission of the Drude component in the calculation. Whereas the GGA + SOC calculation reproduces most peaks below 3 eV, the GGA calculation fails to reproduce the experimental peaks around 0.4 and 2.0 eV. Particularly, the lowest peak in $\sigma_{1b}(\omega)$ corresponds to the transition between the two bands along the UR, which are branched off from the degenerate bands in the absence of SOC. Its peak energy (∼0.4 eV) is very consistent with the known value of SOC (∼0.5 eV) in iridates. Therefore, we concluded that SOC plays an important role to determine the electronic structure of IrO_2, especially near E_F.

C. X-ray-absorption spectroscopy: Orbital character of an empty state near E_F

It is still unclear whether metallic IrO_2 has a $J_{\mathrm{eff}} = 1/2$ ground state near E_F. Note that $J_{\mathrm{eff}} = 1/2$ can be represented by a combination of three t_{2g} orbitals $[\mp\frac{1}{\sqrt{3}}(|d_{xy} \pm 1/2\rangle \pm |d_{yz} \mp 1/2\rangle + i|d_{zx} \mp 1/2\rangle)]$ [1]. So this ground state should be formed with equal contributions of three t_{2g} orbitals d_{xy}, d_{yz}, and d_{zx}. To check the possible formation of the $J_{\mathrm{eff}} = 1/2$ state, we investigated orbital characters of IrO_2 near E_F by using O 1s XAS measurements. The O 1s spectra reflect the transitions from the O 1s core level to the unoccupied O 2p states that are hybridized with Ir 5d orbitals. Since the hybridization varies depending on the extended nature of the d orbitals, the polarized XAS spectra can probe the participation of each t_{2g} orbital in the unoccupied state [37–39].

Figure 3(a) shows the experimental geometry of our XAS measurements, where π and σ polarizations were parallel with respect to the c and b axes, respectively. Figure 3(b) displays the π- and σ-polarization O 1s XAS spectra from 528 to 536 eV, which are normalized by the data at a higher-energy region. The O 1s XAS spectra display a sharp peak denoted by α in Fig. 3(b), followed by two broad peaks denoted by β and γ, respectively. Peak α represents the unoccupied O 2p states hybridized with the Ir t_{2g} orbital, whereas peaks β and γ represent those hybridized with e_g orbitals. These spectra show that t_{2g} and e_g states are well separated above E_F. We found that the orbital character of the empty state

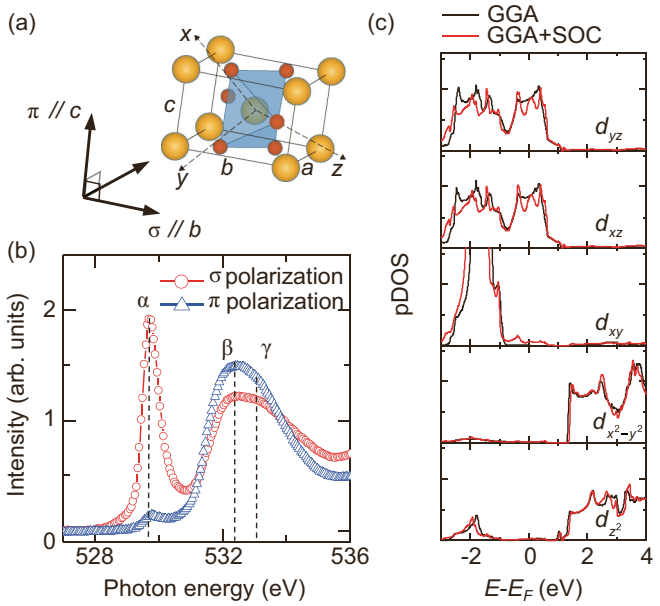

FIG. 3. (a) Indication of sample orientation and polarized light direction. π- and σ-polarization light are parallel to the c and b axes, respectively. (b) O $1s$ polarization-dependent x-ray absorption spectroscopy of IrO_2 grown on a (100) TiO_2 substrate. Red solid circles and blue solid triangles represent σ-polarization and π-polarization spectra, respectively. (c) Projected density of state (pDOS) of d orbitals of IrO_2. The black solid line and the red solid line represent pDOS calculated using GGA and GGA + SOC, respectively.

near E_F is not consistent with the formation of the $J_{\text{eff}} = 1/2$ state. Note, that peak α shows strong polarization dependence: the intensity of π polarization becomes strongly suppressed compared to that of σ polarization. The intensity ratio of peak α in π and σ polarizations is estimated to be $I_\pi/I_\sigma = 0.07$. To understand the large polarization dependence, we evaluated the intensity ratio in π and σ polarizations for the pure $J_{\text{eff}} = 1/2$ orbital states. Since the peak intensities reflect the directional hybridization between O $2p$ and Ir $5d$ orbitals, we calculated their strength by using the Slater-Koster interatomic matrix [40]. We found that the intensity ratio I_π/I_σ should be about 2.9 for the $J_{\text{eff}} = 1/2$ state. This value is much higher than the experimental value of $I_\pi/I_\sigma = 0.07$.

The pDOS of Ir d orbitals also confirms that the orbital character of IrO_2 does not follow the $J_{\text{eff}} = 1/2$ orbital picture. Figure 3(c) shows the pDOS of Ir d orbitals in GGA and GGA + SOC calculations. In GGA, two t_{2g} orbitals d_{xz} and d_{yz}, are responsible for most of the electron density near E_F. There exists a small peak structure near E_F around 0.5 eV. Note that this structure can originate from the flat band dispersion near E_F, along the ZU line in Fig. 2(e) formed due to SOC. However, in both GGA and GGA + SOC calculations, the d_{xy} orbital has most of its electron density on 2.0 eV below E_F. The energy difference between the d_{xy} and the other d orbitals should be originated from their bonding nature. In the rutile structure, the IrO_6 octahedra have edge sharing, and the d_{xy} orbital lies within the plane formed by the shared edges and has little mixing with the O $2p$ orbitals [41]. On the other hand, the d_{xz} and d_{yz} orbitals lie perpendicular to the octahedra-edge sharing plane and have a strong π bonding with O $2p$ orbitals. The resulting energy difference is about 2 eV, much larger than the SOC energy. Therefore, the $J_{\text{eff}} = 1/2$ state cannot be formed in IrO_2.

It was experimentally reported that IrO_2 has a large branching ratio of about 7 in Ir L-edge XAS [19,42]. They suggested that the large branching ratio might come from the formation of the $J_{\text{eff}} = 1/2$ state. However, our observation of the simple π-bonding states with d_{xz} and d_{yz} orbitals near E_F seems to be inconsistent with their results. It should be noted that large $\langle L \cdot S \rangle$ values do not necessarily have to come from the $J_{\text{eff}} = 1/2$ state. Although SOC is not sufficient to form the $J_{\text{eff}} = 1/2$ state in IrO_2, SOC might be able to mix the π-bonding d_{yz} and d_{zx} orbitals to result in the observed large $\langle L \cdot S \rangle$ values. To confirm this intriguing possibility, some more systematic investigations, including resonant inelastic x-ray scattering or polarization-dependent Ir L-edge XAS, are desirable.

IV. OUTLOOK AND CONCLUSION

At this point, let us revisit the controversies related to SOC in IrO_2. First, contrary to our finding that the $J_{\text{eff}} = 1/2$ state cannot be formed in IrO_2, there have been some studies that claimed the existence of this novel state in the metallic compound [20,21]. Note that all of these studies were based on an atomic Hamiltonian. So the inconsistency might come from the fact that they did not properly consider the bonding nature of rutile structures in IrO_2, which was described in Sec. III C. As shown in Fig. 3(c), the bonding nature moves the d_{xy} orbital state far below E_F, i.e., about 2 eV, making it difficult to form the $J_{\text{eff}} = 1/2$ state. Second, let us discuss the importance of SOC in IrO_2. There have been experimental studies which have good agreement on the electronic structure when SOC is turned on. They claimed the importance of SOC by measuring photoemission [15,18], specific heat [13], and optical properties [16,17]. However, by using the density functional calculations, other groups claimed that SOC effects are negligible in the density of states [27,28]. Later, hard-x-ray photoelectron spectroscopy experiments supported such a claim [26]. As shown in Fig. 3(c), the SOC effects in pDOS are quite small except in the region close to E_F. And the band dispersion, shown in Figs. 2(d) and 2(e), also shows that the electronic structural changes due to the SOC should occur close to E_F. Away from E_F, SOC effects will become quite small. Therefore, SOCs should play important roles mainly in physical properties that are determined by the Fermi-surface topology and/or electronic states near E_F.

To summarize, our optical conductivity measurements and the GGA + SOC calculation showed that SOC has an effect on the band-structure formation of IrO_2, close to E_F. However, O $1s$ XAS results and pDOS analysis of Ir d orbitals suggest that the $J_{\text{eff}} = 1/2$ state no longer exists in metallic IrO_2. Maintaining its metallic state with reasonably strong SOC, IrO_2 epitaxial thin films provide a sufficient environment for electronic transport applications, such as highly sensitive spin detection devices [8].

ACKNOWLEDGMENTS

This work was supported by IBS-R009-D1. Experiments at the PLS were supported, in part, by MSIP and POSTECH. S.C.C. was supported by the NRF (Grant No. 2014R1A1A1003676). We highly appreciate a helpful discussion with S.K. Panda, especially for providing us with his theoretical results on electronic structures and optical conductivities. We also acknowledge fruitful discussions with M. Kim.

[1] B. J. Kim, H. Jin, S. J. Moon, J.-Y. Kim, B.-G. Park, C. S. Leem, J. Yu, T. W. Noh, C. Kim, S.-J. Oh, J.-H. Park, V. Durairaj, G. Cao, and E. Rotenberg, Phys. Rev. Lett. **101**, 076402 (2008).

[2] B. J. Kim, H. Ohsumi, T. Komesu, S. Sakai, T. Morita, H. Takagi, and T. Arima, Science **323**, 1329 (2009).

[3] S. J. Moon, H. Jin, W. S. Choi, J. S. Lee, S. S. A. Seo, J. Yu, G. Cao, T. W. Noh, and Y. S. Lee, Phys. Rev. B **80**, 195110 (2009).

[4] A. Shitade, H. Katsura, J. Kuneš, X.-L. Qi, S.-C. Zhang, and N. Nagaosa, Phys. Rev. Lett. **102**, 256403 (2009).

[5] D. Pesin and L. Balents, Nat. Phys. **6**, 376 (2010).

[6] W. Witczak-Krempa, G. Chen, Y. B. Kim, and L. Balents, Annu. Rev. Condens. Matter Phys. **5**, 57 (2014).

[7] G. Jackeli and G. Khaliullin, Phys. Rev. Lett. **102**, 017205 (2009).

[8] K. Fujiwara, Y. Fukuma, J. Matsuno, H. Idzuchi, Y. Niimi, Y. Otani, and H. Takagi, Nat. Commun. **4**, 2893 (2013).

[9] M. Uchida, W. Sano, K. S. Takahashi, T. Koretsune, Y. Kozuka, R. Arita, Y. Tokura, and M. Kawasaki, Phys. Rev. B **91**, 241119 (2015).

[10] W. D. Ryden and A. W. Lawson, J. Chem. Phys. **52**, 6058 (1970).

[11] W. D. Ryden, A. W. Lawson, and C. C. Sartain, Phys. Rev. B **1**, 1494 (1970).

[12] W. D. Ryden, W. A. Reed, and E. S. Greiner, Phys. Rev. B **6**, 2089 (1972).

[13] J. E. Graebner, E. S. Greiner, and W. D. Ryden, Phys. Rev. B **13**, 2426 (1976).

[14] L. F. Mattheiss, Phys. Rev. B **13**, 2433 (1976).

[15] R. R. Daniels, G. Margaritondo, C. A. Georg, and F. Lévy, Phys. Rev. B **29**, 1813 (1984).

[16] A. K. Goel, G. Skorinko, and F. H. Pollak, Phys. Rev. B **24**, 7342 (1981).

[17] W. S. Choi, S. S. A. Seo, K. W. Kim, T. W. Noh, M. Y. Kim, and S. Shin, Phys. Rev. B **74**, 205117 (2006).

[18] G. K. Wertheim and H. J. Guggenheim, Phys. Rev. B **22**, 4680 (1980).

[19] J. P. Clancy, N. Chen, C. Y. Kim, W. F. Chen, K. W. Plumb, B. C. Jeon, T. W. Noh, and Y.-J. Kim, Phys. Rev. B **86**, 195131 (2012).

[20] Y. Hirata, K. Ohgushi, J.-i. Yamaura, H. Ohsumi, S. Takeshita, M. Takata, and T.-h. Arima, Phys. Rev. B **87**, 161111 (2013).

[21] S. K. Panda, S. Bhowal, A. Delin, O. Eriksson, and I. Dasgupta, Phys. Rev. B **89**, 155102 (2014).

[22] J. S. de Almeida and R. Ahuja, Phys. Rev. B **73**, 165102 (2006).

[23] D. A. Zocco, J. J. Hamlin, B. D. White, B. J. Kim, J. R. Jeffries, S. T. Weir, Y. K. Vohra, J. W. Allenv, and M. B. Maple, J. Phys.: Condens. Matter **26**, 255603 (2014).

[24] M. K. Vamshi, S. Nishimoto, V. Yushankhai, A. Stoyanova, H. Kandpal, C. Sungkyun, R. Coldea, I. Rousochatzakis, L. Hozoi, and B. Jeroen van den, New J. Phys. **16**, 013056 (2014).

[25] C. H. Sohn, H. S. Kim, T. F. Qi, D. W. Jeong, H. J. Park, H. K. Yoo, H. H. Kim, J. Y. Kim, T. D. Kang, D.-Y. Cho, G. Cao, J. Yu, S. J. Moon, and T. W. Noh, Phys. Rev. B **88**, 085125 (2013).

[26] J. M. Kahk, C. G. Poll, F. E. Oropeza, J. M. Ablett, D. Céolin, J. P. Rueff, S. Agrestini, Y. Utsumi, K. D. Tsuei, Y. F. Liao, F. Borgatti, G. Panaccione, A. Regoutz, R. G. Egdell, B. J. Morgan, D. O. Scanlon, and D. J. Payne, Phys. Rev. Lett. **112**, 117601 (2014).

[27] M. S. Miao and R. Seshadri, J. Phys.: Condens. Matter **24**, 215503 (2012).

[28] Y. Ping, G. Galli, and W. A. Goddard, J. Phys. Chem. C **119**, 11570 (2015).

[29] C. C. Homes, M. Reedyk, D. A. Cradles, and T. Timusk, Appl. Opt. **32**, 2976 (1993).

[30] M. A. El Khakani, M. Chaker, and E. Gat, Appl. Phys. Lett. **69**, 2027 (1996).

[31] B. R. Chalamala, Y. Wei, R. H. Reuss, S. Aggarwal, B. E. Gnade, R. Ramesh, J. M. Bernhard, E. D. Sosa, and D. E. Golden, Appl. Phys. Lett. **74**, 1394 (1999).

[32] J. Hämäläinen, M. Kemell, F. Munnik, U. Kreissig, M. Ritala, and M. Leskelä, Chem. Mater. **20**, 2903 (2008).

[33] S.-W. Kim, S.-H. Kwon, D.-K. Kwak, and S.-W. Kang, J. Appl. Phys. **103**, 023517 (2008).

[34] C. Wang, Y. Gong, Q. Shen, and L. Zhang, Appl. Surf. Sci. **253**, 2911 (2006).

[35] P. C. Liao, W. S. Ho, Y. S. Huang, and K. K. Tiong, J. Mater. Res. **13**, 1318 (1998).

[36] Y. Liu, H. Masumoto, and T. Goto, Mater. Trans. **45**, 3023 (2004).

[37] H.-J. Noh, S. J. Oh, B. G. Park, J. H. Park, J. Y. Kim, H. D. Kim, T. Mizokawa, L. H. Tjeng, H. J. Lin, C. T. Chen, S. Schuppler, S. Nakatsuji, H. Fukazawa, and Y. Maeno, Phys. Rev. B **72**, 052411 (2005).

[38] T. Mizokawa, L. H. Tjeng, G. A. Sawatzky, G. Ghiringhelli, O. Tjernberg, N. B. Brookes, H. Fukazawa, S. Nakatsuji, and Y. Maeno, Phys. Rev. Lett. **87**, 077202 (2001).

[39] W. B. Wu, D. J. Huang, J. Okamoto, A. Tanaka, H. J. Lin, F. C. Chou, A. Fujimori, and C. T. Chen, Phys. Rev. Lett. **94**, 146402 (2005).

[40] J. C. Slater and G. F. Koster, Phys. Rev. **94**, 1498 (1954).

[41] J. B. Goodenough, J. Solid State Chem. **3**, 490 (1971).

[42] D.-Y. Cho, J. Park, J. Yu, and J.-G. Park, J. Phys.: Condens. Matter **24**, 055503 (2012).